SPATIOTEMPORAL CHANGES OF EXTREME TEMPERATURES IN THE PAST 49 YEARS AND THEIR RELATIONSHIP WITH THE ENSO IN SOUTHWESTERN CHINA

CHEN, Z. F.[1,2] – LI, X. H.[1,*] – WANG, L.[1]

[1]*Plateau Atmosphere and Environment Key Laboratory of Sichuan Province, School of Atmospheric Sciences, Chengdu University of Information Technology, Chengdu 610225, Sichuan, China*

[2]*Shiyan Meteorological Bureau, Shiyan 442000, Hubei, China*

**Corresponding author*
e-mail: lixiehui325328@163.com; phone: +86-28-8563-4698

(Received 15th Mar 2021; accepted 19th Jul 2021)

Abstract. In the present research, spatiotemporal changes of extreme temperatures in Southwestern China as well as their relationship with the El Niño–Southern Oscillation (ENSO) events were determined for the 1969 to 2017 period using the Mann-Kendall test, the Sen's slope estimator, and the empirical orthogonal function (EOF) analysis. For this purpose, daily temperature data of 93 weather stations and 17 extreme temperature indices (ETIs) were analyzed. Our results suggested that: (1) during the past 49 years, ETIs showed a warming trend in Southwestern China, and differences in warming trends were observed in different geographical regions. (2) In the 1990s and early 21st century (2001-2011), abrupt extreme temperature changes were observed. (3) Results of the EOF analysis also indicated abrupt changes in extreme temperature indices. The regions susceptible to changes in the number of ice days (ID) were the Hengduan Mountains and part of the Yunnan-Guizhou Plateau. The high-value midpoints of summer days (SU) were found in the Zoige Plateau, Sichuan Basin, and part of the Yunnan-Guizhou plateau. (4) The ETIs were closely related to the ENSO events. The extreme cold indices were more significantly influenced by La Niña, and the extreme warm indices were more susceptible to El Niño events.

Keywords: *extreme temperature indices, mutation test, Sen's slope estimator, EOF analysis, multiple variation analysis, SOI, ONI*

Introduction

Since the First World Climate Conference (FWCC) held in Geneva in 1979, global warming has been an important topic worldwide. In 2014, the Fifth Assessment Report of the Intergovernmental Panel on Climate Change (IPCC) stated that in the past 130 years, the global temperature increased by 0.65~1.06 °C. In addition, as the warming trend continues, extreme temperatures occur more frequently and for longer periods of time. Different studies have shown that climate warming has changed the spatiotemporal distributions of water resources, leading to more severe and frequent occurrences of related natural disasters, such as droughts and floods. Both, experimental observations and modeling results, have indicated that the ENSO events are also influenced by global warming, with a significant increase in frequency and intensity. Abnormal climate phenomena such as floods in the south and droughts in the north and warmer winters and cooler summers occur as a result of ENSO (IPCC, 2013; Gao et al., 2017; Qiu, 2013). Extreme climate events have given rise to disastrous environmental and socio-economic consequences in many regions, drawing the attention of the public, government, and academics (Gao and Xie, 2016; An et al., 2019).

In the early 21st century, global warming has caused a dramatic increase in both, the frequency and intensity of extreme weather and climate events. Extreme temperature events

http://www.aloki.hu ● ISSN 1589 1623 (Print) ● ISSN 1785 0037 (Online)
DOI: http://dx.doi.org/10.15666/aeer/2002_11131138

are considered the main signs of global warming, and their effects have been observed all over the world. Alexander et al. (2006), Ding et al. (2018) and Zhao et al. (2016, 2017) indicated that global warming has significantly decreased the number of cold nights and increased the number of warm nights in most parts of the world. In the past decades, the frequency of global heat and cold wave events has increased by 2.7 and 6.4 times, respectively (Karl et al., 1991; Cui et al., 2018). According to Diffenbaugh et al. (2017) during historical records, over 80% of the observed regions worldwide displayed a significant increase in the annual number of hottest months and the annual number of hottest days. In addition, model results have also indicated that, for a given area, historical climate forcing increased the probability of observing the driest year and wettest 5-d period at 57% and 41%, respectively. Grotjahn et al. (2016) applied the peaks-over-threshold (POT) method to indirectly determine the generalized extreme value (GEV) in North America. The results showed that the broadest region of warming occurred in the cold tail of the minimum temperature distribution. In some regions of North America, an increasing warming trend was observed (90% confidence interval). Similar results have been reported for China (Zhao et al., 2016, 2017), where intensities were comparable. However, opposite trends for cold night index and warm night index were observed in most parts of China, which indicated a good symmetry. The diurnal temperature change displayed considerable asymmetry, with small diurnal temperature range (DTR). This phenomenon affects the variation of extreme temperatures and accelerates water circulation. In consequence, water resources distribution is also affected (Yang et al., 2010; Chen and Min, 2017; Li et al., 2019). In this context, Pi et al. (2020) identified an abrupt climate change in the arid regions of Northwestern China, with increasing temperatures. The number of summer days (SU25), warm days (TX90p), warm nights (TN90p), and warm spell duration index (WSDI) significantly increased. The increasing rate was 2.27, 1.49, 3, and 2.28 d/10a, respectively. On the other hand, the number of frost days (FD), cold days (TX10p), cold nights (TN10p), and cold spell duration index (CSDI) significantly decreased at a rate of -3.71, -0.86, -1.77, and -0.76 d/10a, respectively. Tong et al. (2020) determined that the maximum and minimum temperatures increased either within the whole Beijing-Tianjin-Hebei Region (BTHR) or locally. The frequency of extreme heat also increased, while the frequency of cold weather decreased.

The warming trend of atmosphere and ocean significantly influences the air-sea interaction (L'Heureux et al., 2017). In this context, ENSO events are considered abnormal phenomena and strong signals of the interaction between the tropical oceans and atmosphere, and they exert a significant impact on temperature in many regions of the world. They also vary in intensity and stability, which results in notable regional features (Yang et al., 2013). For example, in 1982 and 1997 two extreme El Niño events occurred. They are known as the strongest ones of this type ever recorded in history. In each event, the ocean surface temperature in the eastern equatorial Pacific exceeded 28 ℃. These two El Niño events caused an economic loss between 20 and 35-45 billion US dollars each worldwide, and claimed the lives of over 20 thousand people (Shi, 2017; Glantz et al., 1998; Sponberg, 1990). Therefore, the relationship between the ENSO events and the increased intensity and frequency of extreme temperature events has also become one of the major research interests in this area of knowledge (An et al., 2019; Vincent and Mekis, 2006; Choi et al., 2009). In this context, Wang et al. (2017) found out that, from 1961 to 2012, the ENSO events affected winter temperatures in Northern China by modulating the atmospheric circulation over the North Atlantic area. This feature changed the convective transport in zonal temperatures in the mid and high latitudes of Eurasia and the intensity of

http://www.aloki.hu ● ISSN 1589 1623 (Print) ● ISSN 1785 0037 (Online)
DOI: http://dx.doi.org/10.15666/aeer/2002_11131138

Siberian High. The El Niño events caused a decrease in the daily mean temperature of Northeastern China and an increase in the frequency of extreme low temperature events. Lim and Schubert (2011) showed that, as compared with El Niño, La Niña phenomenon played a more critical role in causing more frequent extreme climate events. ENSO offered a reasonable explanation for the upper temperature limit, but not for the lower temperature limit.

Southwestern China has a subtropical monsoon climate, where the annual mean temperature is 14~24 ℃ (Zhao, 1997). In the past 53 years (1960-2012), major natural disasters in Southwestern China have included frequent droughts (Wang et al., 2014a). Data indicated that Southwestern China was hit by extreme droughts in the periods 2006-2007 and 2009-2010. In addition, Sichuan and part of Chongqing were affected by extreme droughts from 2006 to 2007. The cropping area slightly affected by droughts in Chongqing was 1.327 million ha, which represented a direct economic loss of 9.07 billion RMB. In addition, the cropping area moderately affected by droughts in Sichuan was 1.166 million ha. The direct economic loss produced by summer droughts was 12.57 billion RMB (China Meteorological Disaster Yearbook, 2007). A rare extreme drought hit Southwestern China from 2009 to 2010 affecting a population of 51 million, and a cropping area of 6.25 million ha (Qiu, 2013). It has been also reported that, in 2006, the southern oscillation index (SOI) reached a value of -0.28. In addition, in the year of 2007, the oceanic Nino index (ONI) was smaller than -0.5 for six months consecutively. Thus, it was concluded that El Niño phenomenon occurred during the period 2005-2006. In 2009, the ONI was above 0.5 for six months consecutively, while 2010, it increased up to 0.95. This indicated a strong La Niña event. Most studies have concluded that ENSO events are the important external forcing factors causing the two above-mentioned droughts. Later, from October 2012 to the first ten days of March 2013, Yunnan, Sichuan, Chongqing and western Guizhou were also hit by severe droughts, followed by a continuous drought that lasted from autumn to winter and then to spring of the next year. The severe local droughts that occurred from 2015 to 2019 in several stages, caused important economic losses in the provinces of Southwestern China, posing a threat to people’s properties and lives (Wu et al., 2014). In particular, the event that occurred in the Sichuan Basin in the summer of 2017 with prolonged high-temperatures and drought, with the temperature as high as 44 ℃, has been known as the worst since the local meteorological facility initiated operations in 1951. Similarly, the big drought event that occurred in 2017 in Chongqing, caused the longest known summer drought event registered in the meteorological record.

Regarding ETIs, several studies have been conducted in Southwestern China. For example, Yuan et al. (2015) showed that, from 1962 to 2012, FD, TN10p and TX10p significantly decreased at a rate of 2.7, 4.6, and 3.5 d/10a, respectively. It was also determined that TX90p, TN90p, annual minimum value of daily minimum temperature (TNn), and annual minimum value of daily maximum temperature (Txx) increased, at a rate of 3.6, 4.9, 0.4, and 0.1 ℃/10a, respectively. The numbers of extreme high- and low-temperature events in Southwestern China increased and decreased, respectively. Yang et al. (2010) and He et al. (2011) found out that DTR decreased in Southwestern China. In addition, the amplitude increase of extreme low temperatures was considerably larger than that of extreme high temperatures. Furthermore, there was a significant difference in the spatial distribution of extreme temperature events, which highlighted the complexity and distinctiveness of temperature changes in Southwestern China (Yuan et al., 2015; Zhu et al., 2018; Liu and Xu, 2014). Based on existing studies, we selected 17 ETIs and analyzed daily temperatures in the long-term series. Several methods were applied to investigate

http://www.aloki.hu ● ISSN 1589 1623 (Print) ● ISSN 1785 0037 (Online)
DOI: http://dx.doi.org/10.15666/aeer/2002_11131138

spatiotemporal changes and potential trends of extreme temperatures during the past 49 years in Southwestern China. In addition, we identified mutation time of extreme temperature changes, as well as the period of the event and potential influencing factors. We also analyzed the relationship between ETIs and ENSO events in Southwestern China. Our research findings will provide new insights on the development of disaster prevention and relief strategies in events caused by extreme temperatures in Southwestern China.

Study area and data sources

Study area

Southwestern China (21°08’～34°19’ N, 97°21’～110°11’ E) borders with South Central China to the east, Vietnam, Laos and Burma to the south, Tibet Plateau to the west, and Northwestern China to the north. It displays a downwards slopping terrain from the northwest to the southeast. Southwestern China extends over the first and second steps of China’s ladder topography, resulting in a diversity of climate features. According to China’s meteorological and geographical division, the Southwestern Chinese region studied in this paper consists of four provinces and cities: (a) Chongqing city; (b) Sichuan Province; (c) Guizhou Province; and (d) Yunnan Province. In the present research, Southwestern China was divided into the four landform units based on climate and hydrologic conditions, geographical location, as well as altitude from north to south: (a) Zoige Plateau; (b) Hengduan Mountains; (c) Sichuan Basin; and (d) Yunnan-Guizhou Plateau. The Zoige Plateau covers part of Northern Sichuan; Hengduan Mountains cover Western and Southern Sichuan and Northern Yunnan; the Sichuan Basin covers most of Chongqing City and eastern and central Sichuan; and the Yunnan-Guizhou Plateau covers most of Guizhou as well as part of Southern Yunnan.

Due to the special geographical location and complex topographic structure in Southwestern China, the development of urban and social economy in this region is restricted. 1978 was the first year of the implementation of China’s reform and opening up policy. Sichuan (Chongqing was originally under the jurisdiction of Sichuan Province and became a municipality in 1997), Guizhou and Yunnan Province had a total urban population of 14.84 million people, a GDP (Gross Domestic Product) of 30.03 billion yuan, and an urbanization rate of 11.8%. In the latest 20 years, due to the implementation of the western development strategy and the new urbanization road construction, by the end of 2017, the total urban population of the four provinces and cities in Southwestern China was 100.76 million people, the GDP was 8,632.21 billion yuan, and the urbanization rate was 51.89%. Compared with 1978, the urbanization rate increased by 40.09%. In recent years, the urbanization growth rate of the four provinces and cities has exceeded the national urbanization level. By the end of 2017, the total construction land and agricultural land of the four provinces and cities in Southwestern China were 4,388 thousand ha and 96,843.8 thousand ha, respectively, accounting for 3% and 85% of the total land area of the four provinces and cities (China Statistical Yearbook, 2018).

Data sources

Data quality control was performed for the input of daily maximum and minimum temperatures as a previous step for ETIs (Zhang and Yang, 2004). Daily temperature data were obtained from the Meteorological Data Service Center of China (MDSCC) (http://data.cma.cn) for the period 1969 to 2017. Ninety-three weather stations located

http://www.aloki.hu ● ISSN 1589 1623 (Print) ● ISSN 1785 0037 (Online)
DOI: http://dx.doi.org/10.15666/aeer/2002_11131138

in Southwestern China were chosen for the study. Data were processed considering the principles of continuity, homogenisation and longest possible duration. Three quality control methods were used for the treatment of the data: (a) internal consistency check; (b) climate limit check; and (c) station extremum check. Interpolation was performed to fill the data gaps in adjacent stations by using the linear regression method, which ensured that the corrected meteorological data involved high accuracy, homogenisation and continuity (Gao et al., 2017; Zhu et al., 2018). *Figure 1* displays the geographical locations of the 93 studied weather stations in Southwestern China and the digital elevation model (DEM) of the four geographical divisions. *Table 1* shows the distributions of the 93 weather stations in the four geographical divisions. According to *Table 1*, four stations are located in the Zoige Plateau, 22 in the Hengduan Mountains, 23 in Sichuan Basin, and 44 in the Yunnan-Guizhou Plateau. DEM data was obtained from the SRTM data (http://www.cgiar-csi.org/) published by the National Imagery and Mapping Agency. In order to determine the relationship between ETIs and ENSO events, we selected the SOI data from the Climatic Research Unit of the University of East Anglia (http://www.cru.uea.ac.uk/cru/data/soi/) (Wang et al., 2014a). In addition, the ONI data were obtained from the oceanic El Niño index data provided by the NOAA Center for Weather and Climate Prediction and updated once every five years (http://www.cpc.ncep.noaa.gov) (Jiang et al., 2017).

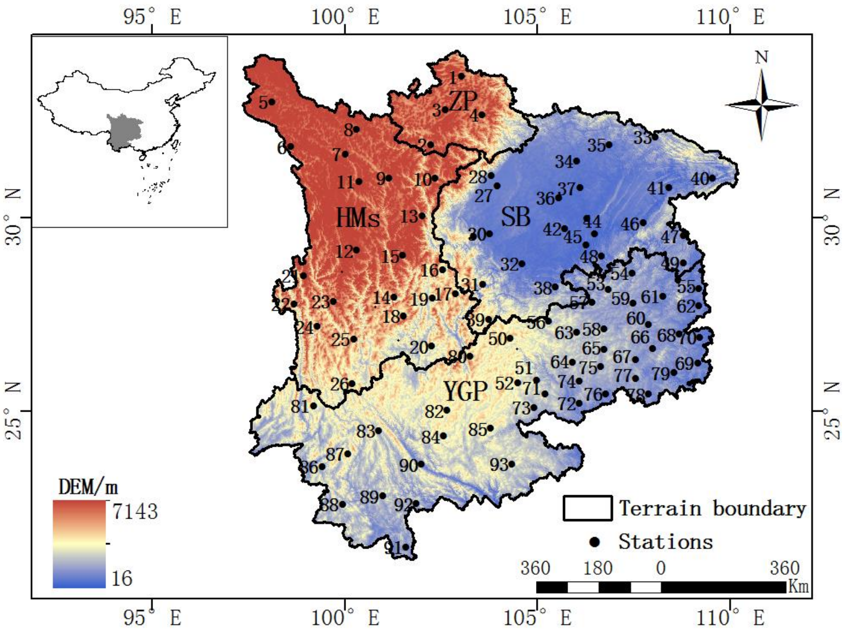

Figure 1. *Topographical division and spatial distribution of weather stations in Southwestern China*

Extreme temperature indices and main research methods

Extreme temperature indices

Numerous studies, both on the global and local scales, have used averages of long- and medium-term low-resolution data to analyze climate change (Croitoru et al., 2013). However, data on changes in ETIs may be more appropriate to use than averages when monitoring, testing, and analyzing the influence of climate change (Peterson et al.,

http://www.aloki.hu ● ISSN 1589 1623 (Print) ● ISSN 1785 0037 (Online)
DOI: http://dx.doi.org/10.15666/aeer/2002_11131138

2008). Herein, 17 ETIs were selected to analyze the features of extreme temperature events in four provinces and cities of Southwestern China (*Table 2*). This was performed in accordance with the Expert Team on Climate Change Detection and Indices (ETCCDI) recommended by the Commission for Climatology (CCI) of World Meteorological Organization (WMO) and Climate Variability and Predictability Program (CLIVAR) (Liu and Xu, 2014). The ETIs were calculated by using the RClimDex (1.0) software developed by Xuebin Zhang and Feng Yang (http://etccdi.pacificclimate.org) (Zhang and Yang, 2004).

Table 1. *Distribution in four terrain zones of 93 weather stations studied in the present research*

Topographical division	Numbers and names of weather stations
Zoige Plateau (ZP)	1 Zoige, 2 MaErKang, 3 HongYuan, 4 SongPan
Hengduan Mountains (HMs)	5 ShiQu, 6 DeGe, 7 GanZi, 8 SeDa, 9 DaoFu, 10 XiaoJin, 11 XinLong, 12 DaoCheng, 13 KangDing, 14 MuLi, 15 JiuLong, 16 YueXi, 17 ZhaoJue, 18 YanYuan, 19 XiChang, 20 HuiLi, 21 DeQin, 22 GongShan, 23 Shangri-La, 24 WeiXi, 25 LiJiang, 26 DaLi
Sichuan Basin (SB)	27 WenJiang, 28 DuJiangYan, 29 EMeiShan, 30 LeShan, 31 LeiBo, 32 YiBin, 33 WanYuan, 34 LangZhong, 35 BaZhong, 36 SuiNing, 37 GaoPing, 38 XuYong, 39 ZhaoTong, 40 FengJie, 41 WanZhou, 42 DaZu, 43 HeChuan, 44 ShaPingBa, 45 JiangJing, 46 FengDu, 47 QianJiang, 48 QiJiang, 49 YouYang
Yunnan-Guizhou Plateau (YGP)	50 WeiNing, 51 PuAn, 52 PanXian, 53 TongZi, 54 ZhengAn, 55 SongTao, 56 BiJie, 57 HuaiRen, 58 XiFeng, 59 MeiTan, 60 YuQing, 61 SiNan, 62 TongRen, 63 QianXi, 64 AnShun, 65 GuiYang, 66 KaiLi, 67 DuYun, 68 SanSui, 69 LiPing, 70 TianZhu, 71 XingRen, 72 WangMo, 73 XingYi, 74 ZiYun, 75 HuiShui, 76 LuoDian, 77 DuShan, 78 LiBo, 79 RongJiang, 80 HuiZe, 81 BaoShan, 82 KunMing, 83 JingDong, 84 YuXi, 85 LuXi, 86 GengMa, 87 LinCang, 88 LanCang, 89 SiMang, 90 YuanJiang, 91 MengLa, 92 JiangCheng, 93 YanShan

Table 2. *List of the 17 selected extreme temperature indices*

Categories	No.	Descriptive names/units	Indices	Definitions
Extreme cold indices	1	Cold spell duration indicator/d	CSDI	Annual count of days with at least 6 consecutive days when TN < 10th percentile
	2	Frost days/d	FD	Annual count when Tn (daily minimum) < 0 ℃
	3	Ice days/d	ID	Annual count when Tx (daily maximum) < 0 ℃
	4	Cool nights/d	TN10p	Number of days when Tn < 10th percentile
	5	Cool days/d	TX10p	Number of days when Tx (daily maximum) < 10th percentile
	6	Average daily minimum temperature/℃	TMINmean	Average Tn
	7	Min Tmin/℃	TNn	Annual minimum value of daily minimum temperature
	8	Min Tmax/℃	TXn	Annual minimum value of daily maximum temperature
Extreme warm indices	9	Warm spell duration indicator/d	WSDI	Annual count of days with at least 6 consecutive days when TX > 90th percentile
	10	Tropical nights/d	TR	Annual count when Tn (daily minimum) > 20 ℃
	11	Summer days/d	SU	Annual count when Tx > 25 ℃
	12	Warm nights/d	TN90p	Number of days when Tn > 90th percentile
	13	Warm days/d	TX90p	Number of days when Tx > 90th percentile
	14	Average daily maximum temperature/℃	TMAXmean	Average Tx
	15	Max Tmin/℃	TNx	Annual maximum value of daily minimum temperature
	16	Max Tmax/℃	TXx	Annual maximum value of daily maximum temperature
	17	Diurnal temperature range/℃	DTR	Monthly mean difference between TX and TN

http://www.aloki.hu ● ISSN 1589 1623 (Print) ● ISSN 1785 0037 (Online)
DOI: http://dx.doi.org/10.15666/aeer/2002_11131138

Main research methods

First, in order to obtain the temporal variation trend of ETIs in the past 49 years, a linear regression analysis was performed using the 17 ETIs. For this purpose, the SPSS (Statistical Program for Social Sciences) was used. Also, a FORTRAN code was written to obtain the univariate linear regression. The linear trend estimation of ETIs at 93 weather stations in Southwestern China was performed by loop computation. The spatial map showing the extreme temperature index spatial trend for the past 49 years in Southwestern China was plotted using ArcGIS. Then, in order to understand the stages of ETIs change, the ETIs trend and year of climate alteration were calculated using the M-K test and the Sen's slope estimator on MATLAB. Later, ETIs were subjected to EOF analysis to determine the spatial ETIs changes. Finally, the relationship between ETIs and ENSO was analyzed using the SOI and ONI. A description of the methods employed in the present study is presented below:

(1) Mann-Kendall test (M-K test): the M-K test is a nonparametric statistical tool that is used to analyze the variation trend of climate and hydrological series over time. This method is also used to identify trends of precipitation and drought frequencies caused by the influence of climate change (Cai, 2016). Samples used for the M-K test may or may not fit a normal distribution. In addition, the samples are not influenced by few outliers. Therefore, the M-K test outperforms other mutation tests for detecting abrupt climate changes (Ma et al., 2018).

For a given time series x, containing n samples, a rank series Sk is constructed as:

$$S_k = \sum_{i=1}^{k} r_i = \begin{cases} 1, & x_i > x_j \\ 0, & x_i \le x_j \end{cases}, \quad j = 1, 2, \ldots, i \tag{Eq.1}$$

where k represents the sample size; r_i is used to determine whether the value at the time i is larger than the value at the time j. According to this, the rank series S_k is the cumulative number of the values, which are larger at the time j than those at the time i.

The statistics is defined as:

$$UF_k = \frac{S_k - E(S_k)}{\sqrt{Var(S_k)}}, \; k = 1, 2, \ldots, n \tag{Eq.2}$$

where:

the mean:
$$E(S_k) = \frac{n(n+1)}{4} \tag{Eq.3}$$

the standard deviation:
$$Var(S_k) = \frac{n(n-1)(2n+5)}{72} \tag{Eq.4}$$

$UF_1 = 0$, $E(S_k)$ and $Var(S_k)$ are the mean and standard deviation of the rank series S_k, respectively; UF_k is the standard normal distribution. The described process is repeated according to the reverse order of the time series x, and $UB_k = -UF_k$. Subsequently, the plotted curves are analyzed. If $UF > 0$, the variable shows an increasing trend. On the other hand, if $UF < 0$, the variable displays a decreasing

http://www.aloki.hu ● ISSN 1589 1623 (Print) ● ISSN 1785 0037 (Online)
DOI: http://dx.doi.org/10.15666/aeer/2002_11131138

trend. In addition, an intersection between the statistic of UF and UB, which lies between the critical lines, corresponds to the start time of climate mutation (i.e., the year of climate mutation).

(2) Sen’s slope estimator: Theil–Sen estimator, also known as Sen’s slope estimator or Kendall robust line-fit method, is used to robustly fit the line to the sampling points distributed on a plane. This method uses the median of all lines’ slopes, which are connected to the paired points. This estimator has proven to be an effective method. For skewed and heteroscedastic data, the Sen’s slope estimator achieves a more clear and accurate result as compared to the non-robust simple linear regression. In terms of statistical power, the Sen’s slope estimator outperforms the non-robust least square method even for the data obeying a normal distribution. Therefore, the Sen’s slope estimator is known as the most popular nonparametric technique for estimating a linear trend. The Sen’s slope estimator is represented by

$$\beta = Median\left(\frac{X_j - X_i}{j - i}\right) \quad j > i = 1, 2, \ldots, n \qquad \text{(Eq.5)}$$

where X_j and X_i are elements of the j and i moments, respectively, in the series to be analyzed. The moment i precedes moment j; $\frac{X_j - X_i}{j-i}$ is the slope between the moments j and i; Median is the median function. When $\beta > 0$, the time series displays an upward trend; when $\beta < 0$, the time series displays a downward trend (Croitoru et al., 2013).

(3) Multiple variation analysis and the determination of years of temperature anomalies: ETIs multiple variation analysis between ETIs and ENSO events provided evidence of the influence of global temperature changes on extreme temperature events in Southwestern China. The composite rate of ETIs was defined as the ratio of mean ETIs value in the years when ENSO occurred to long-term ETIs mean values. Two indices, SOI and ONI, were chosen for comparison and mutual corroboration to determine whether ENSO events occurred. SOI corresponds to the standard deviation of the atmospheric pressure observed in Darwin Island and Tahiti Island. Generally speaking, negative SOI indicates an El Niño event, and positive SOI a La Niña event. ONI is an indicator of the occurrence of an El Niño event based on sea surface temperature anomalies in 1, 2, 3, and 4 regions. Thus, ONI > + 0.5 °C corresponds to an El Niño event. On the other hand, ONI < -0.5 °C indicates a La Niña event.

(4) EOF analysis: EOF, also known as eigenvector analysis (EA) or principal component analysis (PCA), is used to determine structural features of the matrix data by extracting the principal eigenvalues. No established function is used in EOF. In addition, there is no need for a specific function as the basis function in order to carry out the decomposition. EOF analysis decomposes the signals from irregularly distributed stations within a finite region. This method performs a rapid convergence, easily decomposing the information of the variable field into several modes. The spatial structure analyzed by the EOF analysis provides physical information. Because of these benefits, the EOF analysis has become a major tool for analyzing the variable field features in climate change studies. The calculations are performed as follows:

① The anomaly is processed in order to normalize the original data matrix X. Later, the covariance matrix is calculated as S = XX’, where S corresponds to the m×m real symmetric matrix, and m is the number of space points in the variable field.

http://www.aloki.hu ● ISSN 1589 1623 (Print) ● ISSN 1785 0037 (Online)
DOI: http://dx.doi.org/10.15666/aeer/2002_11131138

② The eigenvalue ∧ and eigenvector V of the matrix S are obtained by the eigenvalue and eigenvector method of real symmetric matrix.

③ The matrix ∧ is the diagonal matrix, and the diagonal element is the eigenvalue of XX’, $\lambda = (\lambda_1, \lambda_2, \ldots, \lambda_m)$. The eigenvalues are ranked in descending order: $\lambda_1 \geq \lambda_2 \geq \ldots \geq \lambda_m \geq 0$.

④ The time coefficient matrix T is obtained using T = V’X.

⑤ The variance contribution R_k of each eigenvector and the cumulative variance contribution G of the top p eigenvectors are calculated according to:

$$R_k = \lambda_k \Big/ \sum_{i=1}^{m} \lambda_i \quad k = 1, 2, \ldots, p (p < m) \tag{Eq.6}$$

$$G = \sum_{i=1}^{P} \lambda_i \Big/ \sum_{i=1}^{m} \lambda_i \quad p < m \tag{Eq.7}$$

Results

ETIs variability

Interannual and interdecadal variability

Figure 2 displays the interannual and interdecadal changes of ETIs in Southwestern China from 1969 to 2017. According to the regression analysis performed with data of 93 weather stations, the linear trend rates of the 8 extreme cold indices among the 17 extreme temperature indices indicated an upward temperature trend and a downward trend for the number of cold days. Thus, a warming trend was consistently identified. The interannual change trend rates were -1.1 d/10a (CSDI), -2.34 d/10a (FD), -0.41 d/10a (ID), -3.52 d/10a (TN10p), -1.34 d/10a (TX10p), 0.28 °C/10a (TMINmean), 0.43 °C/10a (TNn), and 0.31 °C/10a (TXn), where $P \leq 0.01$. In addition, the coefficient of determination (R2) for the regression line between TN10p and TMINmean was 0.7, which indicated a good fit. The 8 extreme warm indices and 8 extreme cold indices were validated with each other, all of them indicating a warming trend. The interannual change trend rates were 1.64 d/10a (WSDI), 2.44 d/10a (TR), 0.81 d/10a (SU), 1.87 d/10a (TN90p), 3.09 d/10a (TX90p), 0.22 °C/10a (TMAXmean), 0.20 °C/10a (TNx), and 0.27 °C/10a (TXx). All of them passed the significance test at the 95% confidence interval (CI). A large difference was observed in the amplitude variations between different types of ETIs. Specifically, the difference in amplitude between TN10p and TX90p was higher than that observed between other ETIs. In addition, DTR decreased, indicating a gradual reduction of minimum and maximum temperatures differences. However, the fitting results failed to pass the statistical test, indicating a poor fit. Also, amplitude variations of extreme cold and warm indices were similar, indicating symmetry of the temporal changes of the two types of indices.

Data also indicated that the degree to which warming occurred varied between regions. *Table 3* displays specific change rates for different indices. Data indicated that the mean change rates of the top five extreme cold indices (CSDI, FD, ID, TN10p, and TX10p) in the Zoige Plateau, the Hengduan Mountains, Sichuan Basin, and Yunnan-Guizhou Plateau were -2.68, -2.49, -1.37, and -1.52 d/10a, respectively. The mean change rates of the top five extreme warm indices (WSDI, TR, SU, TN90p, and TX90p)

http://www.aloki.hu ● ISSN 1589 1623 (Print) ● ISSN 1785 0037 (Online)
DOI: http://dx.doi.org/10.15666/aeer/2002_11131138

in the Zoige Plateau, the Hengduan Mountains, Sichuan Basin, and Yunnan-Guizhou Plateau were 1.66, 2.03, 2.58, and 1.57 d/10a respectively. It was also determined that the mean change rates of the last three extreme cold indices (TMINmean, TNn, and TNx) were 0.43, 0.35, 0.30, and 0.34 ℃/10a, which corresponded to the Zoige Plateau, the Hengduan Mountains, Sichuan Basin, and Yunnan-Guizhou Plateau, respectively. Furthermore, the mean change rates of the last three extreme warm indices (TMAXmean, TNx, and TXx), were 0.32, 0.27, 0.28, and 0.18 ℃/10a in the Zoige Plateau, the Hengduan Mountains, Sichuan Basin, and Yunnan-Guizhou Plateau, respectively. Thus, according to the results, the Zoige Plateau was the region were extreme cold indices decreased the most and temperature showed the highest increase. In addition, the indices of extreme warm temperature mostly increased in the Sichuan Basin. As previously stated, the climate change pattern varied across the geographical regions, showing a warming trend.

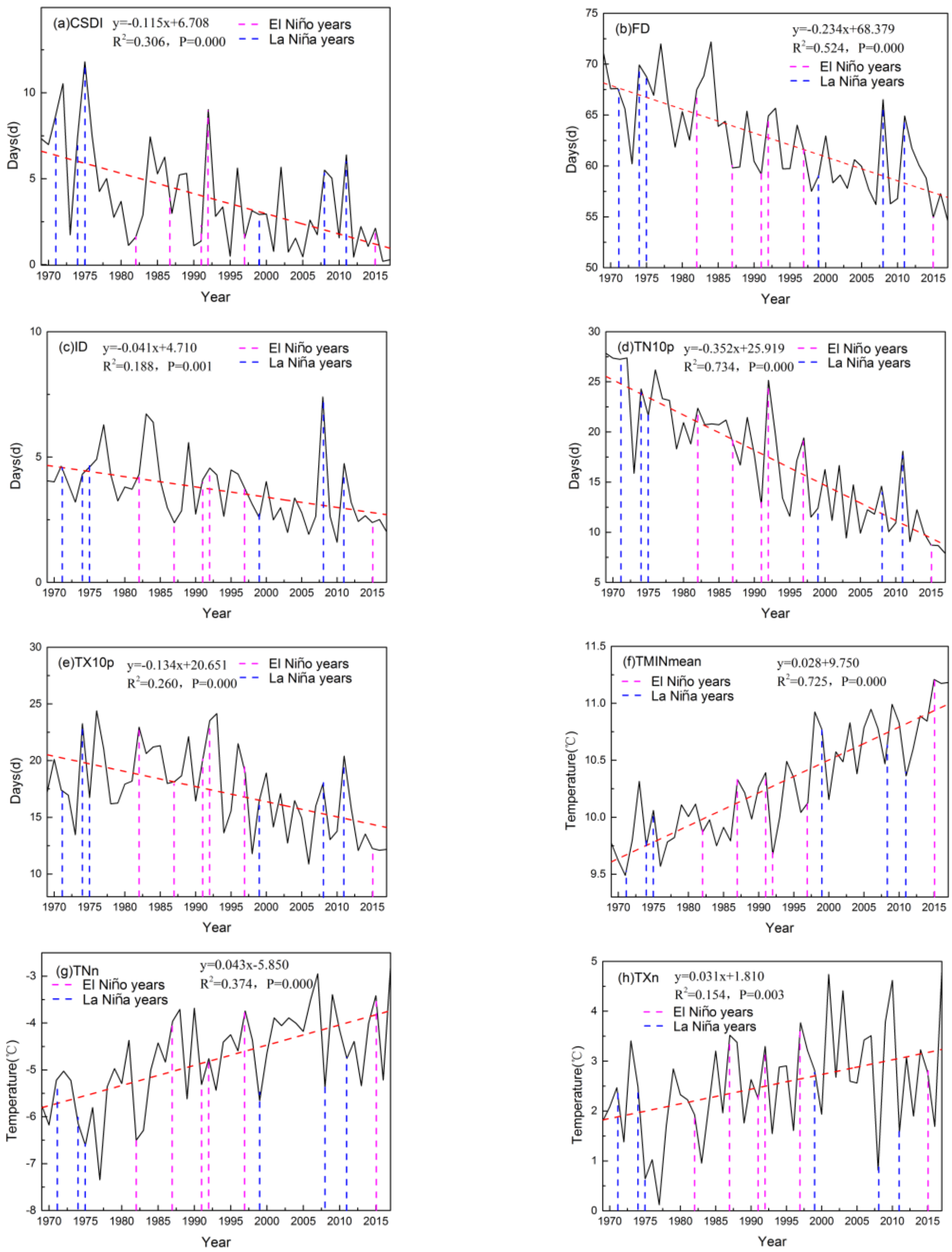

http://www.aloki.hu ● ISSN 1589 1623 (Print) ● ISSN 1785 0037 (Online)
DOI: http://dx.doi.org/10.15666/aeer/2002_11131138

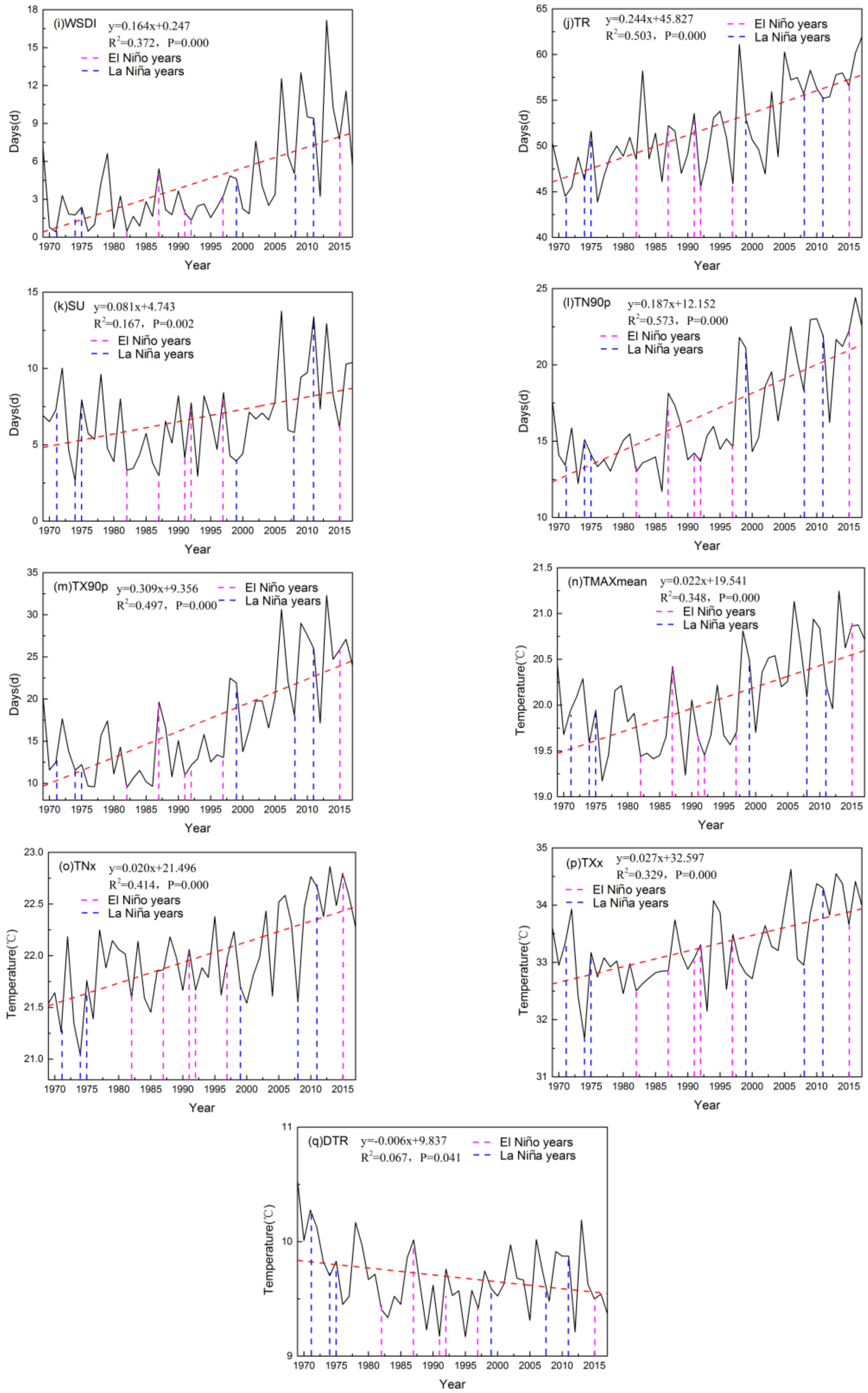

Figure 2. *Time trend of 17 ETIs (referring to Table 2) in Southwestern China from 1969 to 2017*

Results of the comparison between SOI and ONI indicated that the years of strong ENSO events were 1982, 1987, 1991, 1992, 1997, and 2015, while those of strong La Niña events were 1971, 1974, 1975, 1999, 2008, and 2011. Combining this information

http://www.aloki.hu ● ISSN 1589 1623 (Print) ● ISSN 1785 0037 (Online)
DOI: http://dx.doi.org/10.15666/aeer/2002_11131138

with that in *Figure 2*, it was observed that, in some years, ETIs displayed a correspondence to the ENSO events. Thus, in the El Niño years, the value of the extreme cold indices CSDI, FD, ID, TN10p, and TX10p decreased. However, a peak was observed in TMINmean, TNn, and TNx values, indicating an upward trend. The opposite was observed in the La Niña years. In addition, in the El Niño years, a peak occurred in the extreme warm indices, which indicated a warming trend. Thus, the warming trend in Southwestern China presented a certain connection with the ENSO events.

Table 3. *Change rates of 17 ETIs (referring to Table 2) in four different zones*

Division	CSDI (d/10a)	FD (d/10a)	ID (d/10a)	TN10p (d/10a)	TX10p (d/10a)	TMINmean (℃/10a)	TNn (℃/10a)	TXn (℃/10a)	
RP	-0.79	-4.89	-1.65	-4.15	-1.94	0.39	0.55	0.36	
HMs	-1.26	-4.29	-0.89	-4.18	-1.82	0.33	0.42	0.29	
SB	-0.82	-1.51	-0.27	-2.78	-1.47	0.23	0.33	0.35	
YGP	-1.18	-1.85	-0.13	-3.44	-0.98	0.27	0.46	0.28	
Division	**WSDI (d/10a)**	**TR (d/10a)**	**SU (d/10a)**	**TN90p (d/10a)**	**TX90p (d/10a)**	**TMAXmean (℃/10a)**	**TNx (℃/10a)**	**TXx (℃/10a)**	**DTR (d/10a)**
RP	1.75	0	0.02	3.59	2.95	0.3	0.29	0.38	-0.08
HMs	1.95	0.36	0.14	3.95	3.75	0.29	0.24	0.28	-0.05
SB	2.09	2.41	1.68	3.04	3.69	0.26	0.23	0.36	-0.05
YGP	1.29	3.26	0.75	-0.01	2.54	0.16	0.15	0.22	-0.1

Spatial variations characteristics

Figure 3 presents the spatial distribution of the regression coefficients of ETIs obtained at 93 weather stations in Southwestern China for the past 49 years. The spatial change rates and the results of the significance tests are shown in *Table 4*. Results indicated differences in the ETIs change trends as regions varied. Specifically, the top five extreme cold indices showed a downward trend from east to west. Change rates for CSDI, FD, ID, TN10p, and TX10p were -1.15, -2.47, -0.41, -3.52, and -1.34 d/10a, respectively. In the Hengduan Mountains, these five indices dramatically decreased to values of -1.26 d/10a (CSDI), -4.29 d/10a (FD), -0.89 d/10a (ID), -4.18 d/10a (TN10p), and -1.82 d/10a (TX10p). The increase in value and amplitude between these extreme cold indices in the Hengduan Mountains exceeded those observed in other regions. In other words, the warming trend was more severe in high-altitude areas. TMINmean (0.28 ℃/10a), TNn (0.42 ℃/10a), and TXn (0.31 ℃/10a) all showed an upward trend. Moreover, TNn displayed the highest increase in amplitude. Weather stations with a dramatic increase in TNn corresponded to the Hengduan Mountains and the eastern Yunnan-Guizhou Plateau. The highest TNn value, which was 1.30 ℃/10a, was observed at the Shangri-La Station in Yunnan. The maximum positive TXn change rate was observed in Fengjie, Chongqing, with a value of 1.30 ℃/10a. The maximum TMINmean increase was observed in Muli, Sichuan, with a value of 0.9 ℃/10a. Every extreme warm index showed an increasing trend (1.66 d/10a for WSDI, 2.22 d/10a for TR, 0.81 d/10a for SU, 1.83 d/10a for TN90p, 3.13 d/10a for TX90p, 0.22 ℃/10a for TMAXmean, 0.20 ℃/10a for TNx, and 0.28 ℃/10a for TXx). Also, it was determined that the lowest statistical significances were obtained for the upward trend of TNx, and

http://www.aloki.hu ● ISSN 1589 1623 (Print) ● ISSN 1785 0037 (Online)
DOI: http://dx.doi.org/10.15666/aeer/2002_11131138

such a trend was only observed in the Sichuan Basin (0.23 ℃/10a) and northeastern Yunnan-Guizhou Plateau (0.15 ℃/10a). When all the warm extreme indices were considered, Sichuan Basin displayed the most severe warming trend. The temperature extreme occurred more frequently in Fengjie, Chongqing (5.93 d/10a for WSDI, 8.91 d/10a for TX90p, and 0.85 ℃/10a for TMAXmean, all passing the significance test at the 0.01 level), and the weather station in Fengjie displayed the most severe warming trend. In addition, DTR significantly decreased (-0.05 d/10a), indicating a decreasing difference between daytime and nighttime temperatures.

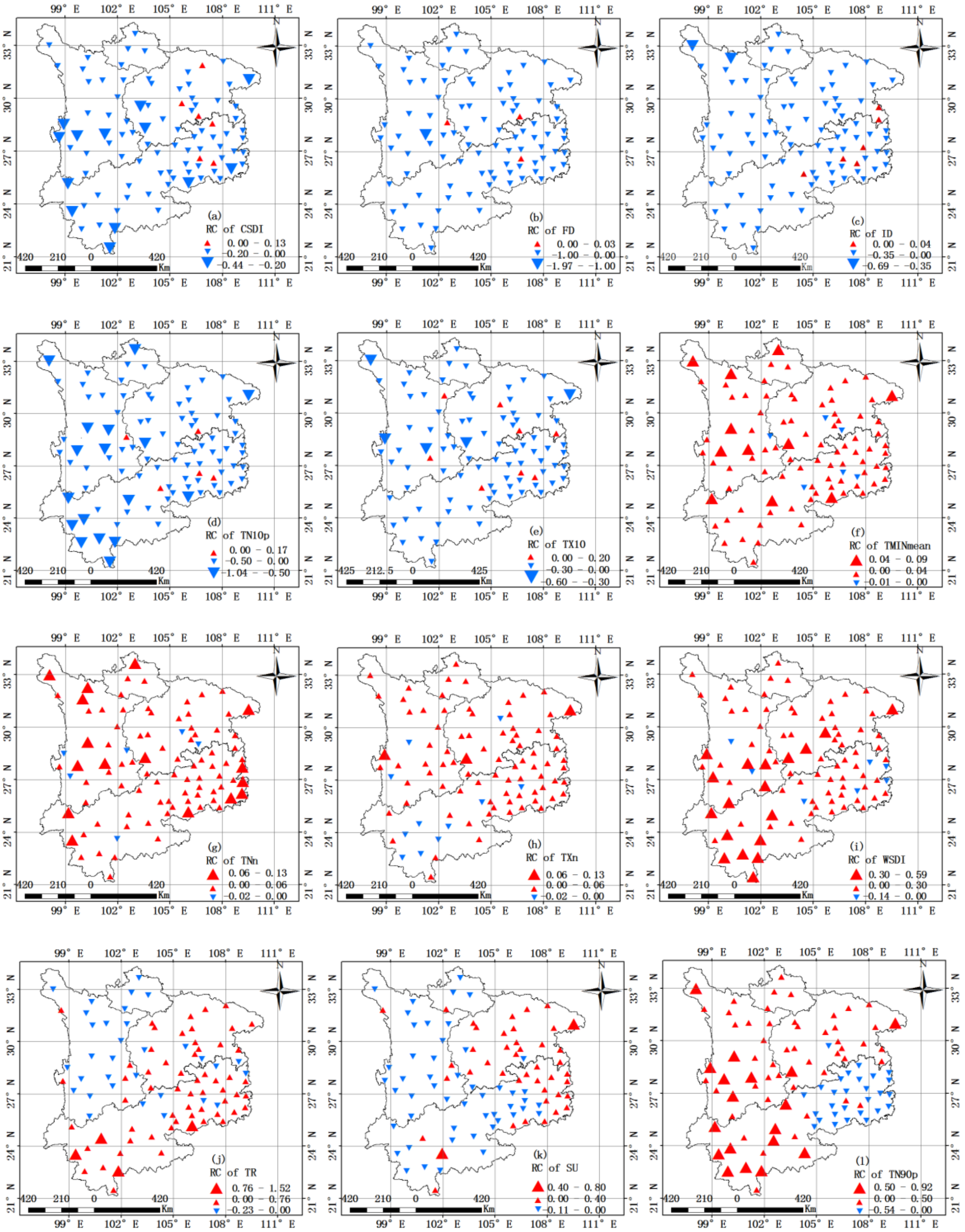

http://www.aloki.hu ● ISSN 1589 1623 (Print) ● ISSN 1785 0037 (Online)
DOI: http://dx.doi.org/10.15666/aeer/2002_11131138

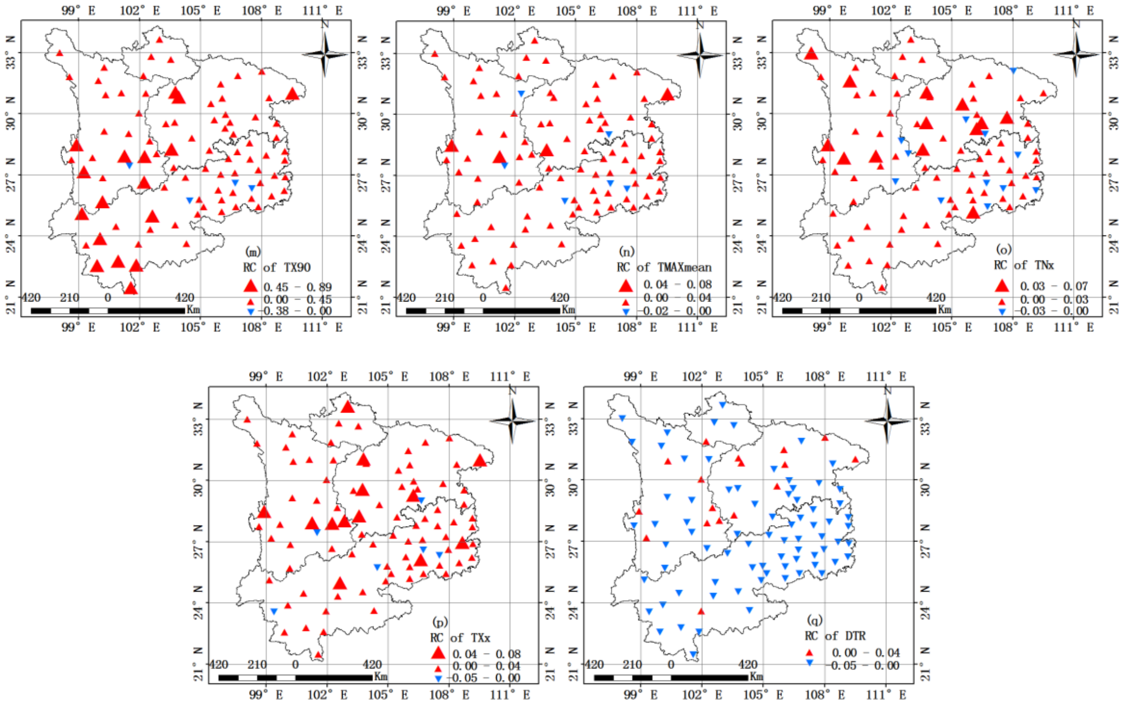

Figure 3. *Spatial change trends of 17 ETIs (referring to Table 2) in Southwestern China from 1969 to 2017*

Table 4. *The spatial change rates and the results of the significance test level in 17 ETIs (referring to Table 2)*

Indices	**CSDI**	**FD**	**ID**	**TN10p**	**TX10p**	**TMINmean**	**TNn**	**TXn**	
Change rates	-0.115	-0.247	-0.041	-0.352	-0.134	0.028	0.043	0.031	
P ≤ 0.01	30.11%	61.29%	50.54%	88.17%	45.16%	90.32%	53.76%	23.66%	
P ≤ 0.05	47.31%	75.27%	51.61%	91.40%	72.04%	91.40%	69.89%	48.39%	
P ≤ 0. 1	58.06%	83.87%	55.91%	92.47%	80.65%	92.47%	82.80%	55.91%	
Indices	**WSDI**	**TR**	**SU**	**TN90p**	**TX90p**	**TMAXmean**	**TNx**	**TXx**	**DTR**
Change rates	0.164	0.244	0.081	0.187	0.309	0.022	0.020	0.027	-0.006
P ≤ 0.01	50.54%	68.82%	58.06%	86.02%	80.65%	72.04%	59.14%	39.78%	39.78%
P ≤ 0.05	55.91%	75.27%	66.67%	90.32%	91.40%	84.95%	65.59%	61.29%	49.46%
P ≤ 0.1	65.59%	82.80%	70.97%	91.40%	92.47%	90.32%	70.97%	69.89%	56.99%

Mutation characteristics

Climate mutation manifests as abrupt changes in the statistical spatiotemporal variability of the climate and is usually indicated by the mutation points (Fu and Wang, 1992). The change trend and mutation points of ETIs were determined by using the M-K test and the Sen's slope estimator to ensure the scientificity and accuracy of the research. These tests were performed using MATLAB. *Table 5* shows the results of the M-K test and Sen's slope estimator of ETIs for the period 1969 to 2017. According to the data shown in *Table 5*, the mutation years of extreme cold indices were identified between the 1990s and early 21st century (2005-2011), while the mutation years of extreme warm indices occurred in the early 21st century (2001-2008). It was also determined that the mutation years of extreme warm indices fell behind those of the extreme cold indices. Combining this information with that in *Figure 2,* it was observed that the number of days of extreme cold indices suddenly decreased in the 1990s, which was accompanied by a significant increase in temperature. Data also indicated that, in the early 21st century, an abrupt change in the extreme warm indices, with a higher number of warm days and temperature increase occurred. The results from the Sen's slope estimator were in accordance with those obtained applying the regression coefficients of interannual and interdecadal ETIs variations. In this case, the change trend was exactly the same. The change trend of the Sen's slope on the UF curve was the same as the trend estimated by the regression coefficient of the interannual and interdecadal changes; however, due to an insignificant change in DTR, the results were the opposite.

Table 5. *M-K test and Sen's slope estimation analysis results of 17 ETIs (referring to Table 2)*

Categories	Indices	M-K test	Sen's slope estimation (time series)	Trend	Sen's slope estimation (UF)	Trend
Extreme cold indices	CSDI	1989, 1992	-0.102	Decline	-0.085	Decline
	FD	1991, 1992, 1993	-0.238	Decline	-0.123	Decline
	ID	1998	-0.043	Decline	-0.100	Decline
	TN10p	1991, 1993	-0.366	Decline	-0.127	Decline
	TX10p	2005, 2007, 2008, 2011	-0.131	Decline	-0.069	Decline
	TMINmean	1996	0.028	Rise	0.154	Rise
	TNn	1986	0.043	Rise	0.113	Rise
	TXn	1986-1987, 1989	0.031	Rise	0.081	Rise
Extreme warm indices	WSDI	2001-2002	0.128	Rise	0.113	Rise
	TR	1998, 1999, 2002	0.231	Rise	0.107	Rise
	SU	2006, 2008	0.077	Rise	0.066	Rise
	TN90p	2002	0.179	Rise	0.157	Rise
	TX90p	2002	0.291	Rise	0.161	Rise
	TMAXmean	2002-2003	0.022	Rise	0.110	Rise
	TNx	2002	0.021	Rise	0.073	Rise
	TXx	2004	0.028	Rise	0.113	Rise
	DTR	1971, 2009-2011, 2012-2013, 2014-2015	-0.005	Decline	0.006	Rise

Figure 4 displays the M-K test curves for 17 ETIs. According to the results, the upper outlier limits of the top five extreme cold indices and DTR passed the significance test at the 95% CI. In addition, the lower outlier limits of other extreme cold indices and most extreme warm indices passed the significance test at the 95% CI. Numerous outliers were observed for CSDI and TNx on the UF curve (*Fig. 4a*), and most of them were located in the tail (on the side of larger values). Since the medians were larger than the means, the UF curve was skewed to the left. The UB curve of TNx (*Fig. 4b*) was skewed to the right, and most outliers displayed small values. Moreover, CSDI, FD, ID and TN10p showed a descending trend, while TX10p only decreased slightly. All upper outlier bounds passed the significance test at the 95% CI. In addition, TMINmean, TNn and TXn showed an upward trend, and their lower outlier limits also passed the significance test. According to *Table 5,* the mutation points occurred in the 1990s. That is, the extreme cold events atypically decreased during this period. Eight extreme warm indices, WSDI, TR, SU, TN90p, TX90p, TMAXmean, TNx, and TXx, showed an increasing trend and their lower outlier limits passed the significance test. The mutation points occurred in the early 21st century. That is, the extreme warm events increased abnormally during this period, and they were accompanied by a very high temperature rise. DTR showed a downward trend,

http://www.aloki.hu ● ISSN 1589 1623 (Print) ● ISSN 1785 0037 (Online)
DOI: http://dx.doi.org/10.15666/aeer/2002_11131138

and the upper limit of the outliers on the UF curve passed the significance test. Since the mutation points occurred in the early 21st century (2009-2015), it was concluded that DTR decreased suddenly at this point in time, indicating smaller differences between daily maximum and minimum temperatures.

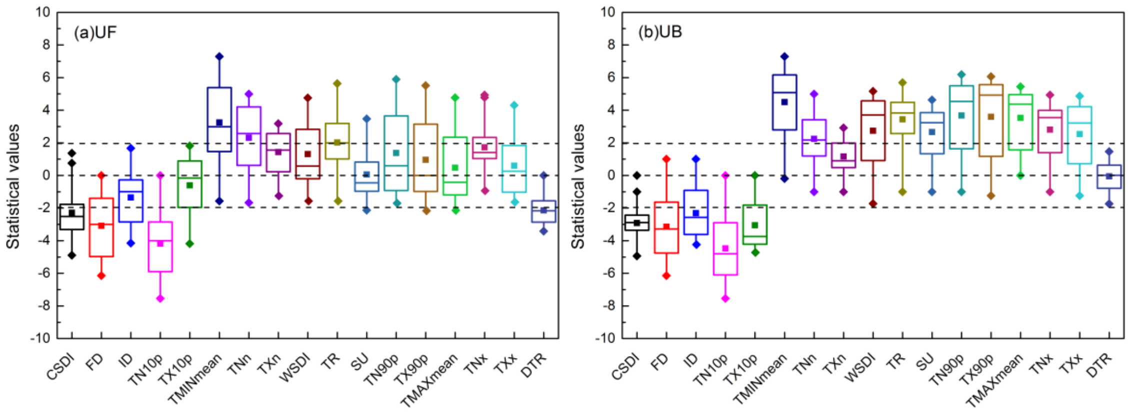

***Figure 4.** M-K inspection box diagrams of 17 ETIs (referring to Table 2)*

EOF analysis

ETIs were extended by using the EOF analysis, and North criterion was used to test the significance. The cumulative variance percent value of the top five loading vectors of ID and SU was up to 90%, which indicated a proper representation of the original vector field. Among the 17 ETIs, the smallest number of loading vectors with the highest cumulative variance contribution rates were those corresponding to ID and SU. Therefore, ID (extreme cold index) and SU (extreme warm index), were chosen for the subsequent EOF analysis. *Table 6* presents the eigenvalues, cumulative variance contribution rates, and the variance contribution rates of the first five modes for ID and SU indices. In both cases, the cumulative variance contribution rates of the two top loading vectors were 75%, approximately. Hence, the top two loading vectors indicated the spatiotemporal changes of ETIs in Southwestern China. In the present research, only the two top loading vectors of the ID and SU indices were analyzed. *Figures 5–6* show the time coefficient series and the spatial distribution modes of the two top loading vectors of ID and SU after EOF analysis, respectively.

***Table 6.** Eigenvalues and variance contribution rates of the first five modes for ID and SU indices*

Variable	Modal	Eigenvalue	Cumulative variance contribution rate	Variance contribution rate
ID	1	35656.14	52.17%	52.17%
	2	14817.06	73.85%	21.68%
	3	6054.771	82.71%	8.86%
	4	3566.85	87.93%	5.22%
	5	1958.087	90.80%	2.87%
SU	1	102025	60.11%	60.11%
	2	26453.18	75.70%	15.59%
	3	12814.79	83.25%	7.55%
	4	5383.14	86.42%	3.17%
	5	3684.315	88.59%	2.171

http://www.aloki.hu ● ISSN 1589 1623 (Print) ● ISSN 1785 0037 (Online)
DOI: http://dx.doi.org/10.15666/aeer/2002_11131138

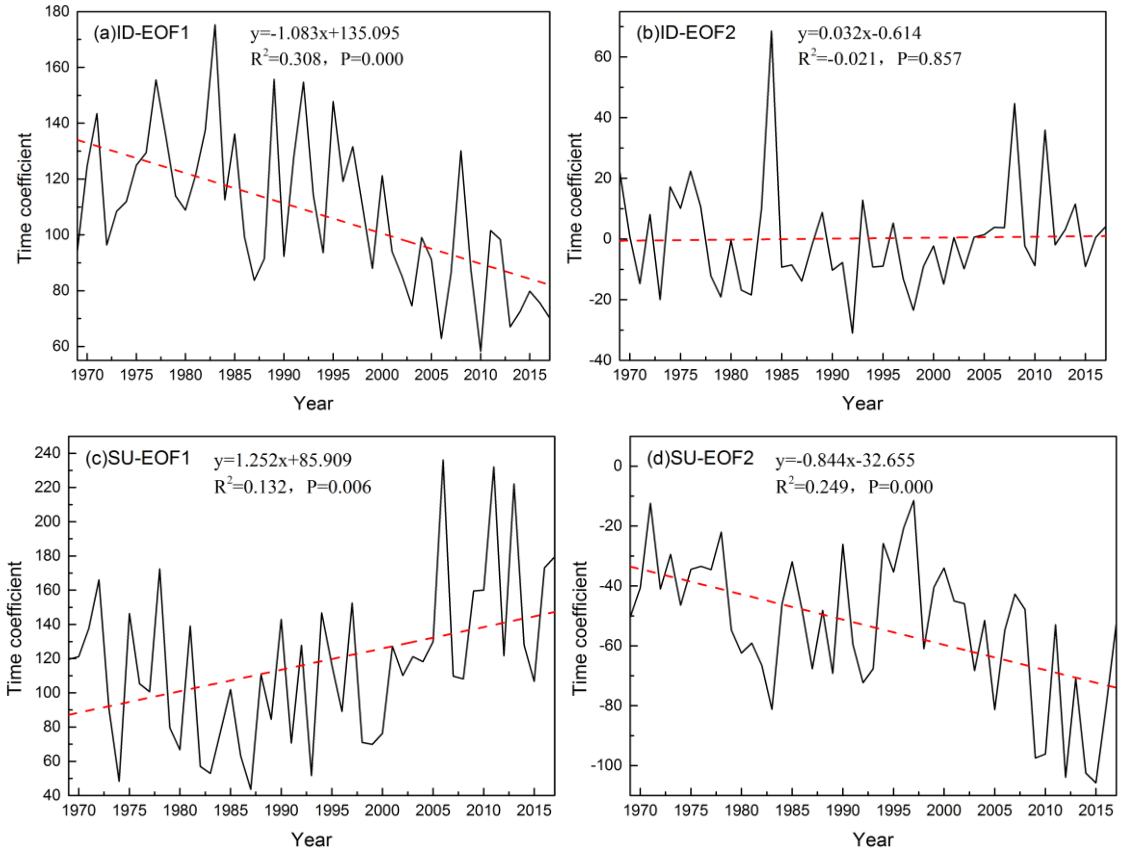

Figure 5. *Temporal EOF variation for ID and SU*

Figure 5 shows that the top one loading vectors of ID and SU were positive values, indicating a positive correlation for both ID and SU in Southwestern China. The change trends for both indices were highly consistent. Results indicated that, for the past 49 years in Southwestern China, ID decreased and SU increased. In addition, around 1990, ID significantly decreased. Moreover, SU suddenly increased in the early 21st century, which indicated the appearance of the mutation point. According to the data presented in *Figure 6*, the first ID mode showed a positive response. Furthermore, a small area in Western Hengduan Mountains and most of the Western Yunnan-Guizhou Plateau presented high loading values. It was also determined that the loading components reached or exceeded values of 0.5. These areas were susceptible to ID changes and the susceptibility decreased from southwest to northeast. Moreover, according to the data displayed in *Figure 5*, ID decreased from southwest to northeast. The percentage of variance of the second ID mode was 21.68% and the loading component was negative in the southwest. This is, the high-value region of the first mode became the low-value region of the second mode. Also, the high-value region of the second mode was positive in the east and northeast. As indicated by the time series data, a downward trend in the western Yunnan-Guizhou Plateau and an upward trend in most of the eastern Yunnan-Guizhou Plateau were observed. The amplitude decreased from west to east; however, no significant difference was observed. The first SU mode displayed a positive response, with a central high-value located in the eastern Zoige Plateau, part of Sichuan Basin, and the central Yunnan-Guizhou Plateau. *Figure 5* also shows that SU significantly increased in these regions, indicating a temperature

http://www.aloki.hu ● ISSN 1589 1623 (Print) ● ISSN 1785 0037 (Online)
DOI: http://dx.doi.org/10.15666/aeer/2002_11131138

increase. The high loading component of the second SU mode corresponded to the central Yunnan-Guizhou Plateau, and the low loading component to the northern Sichuan Basin. Also, as shown by the downward trend in the time series, SU generally decreased from south to north.

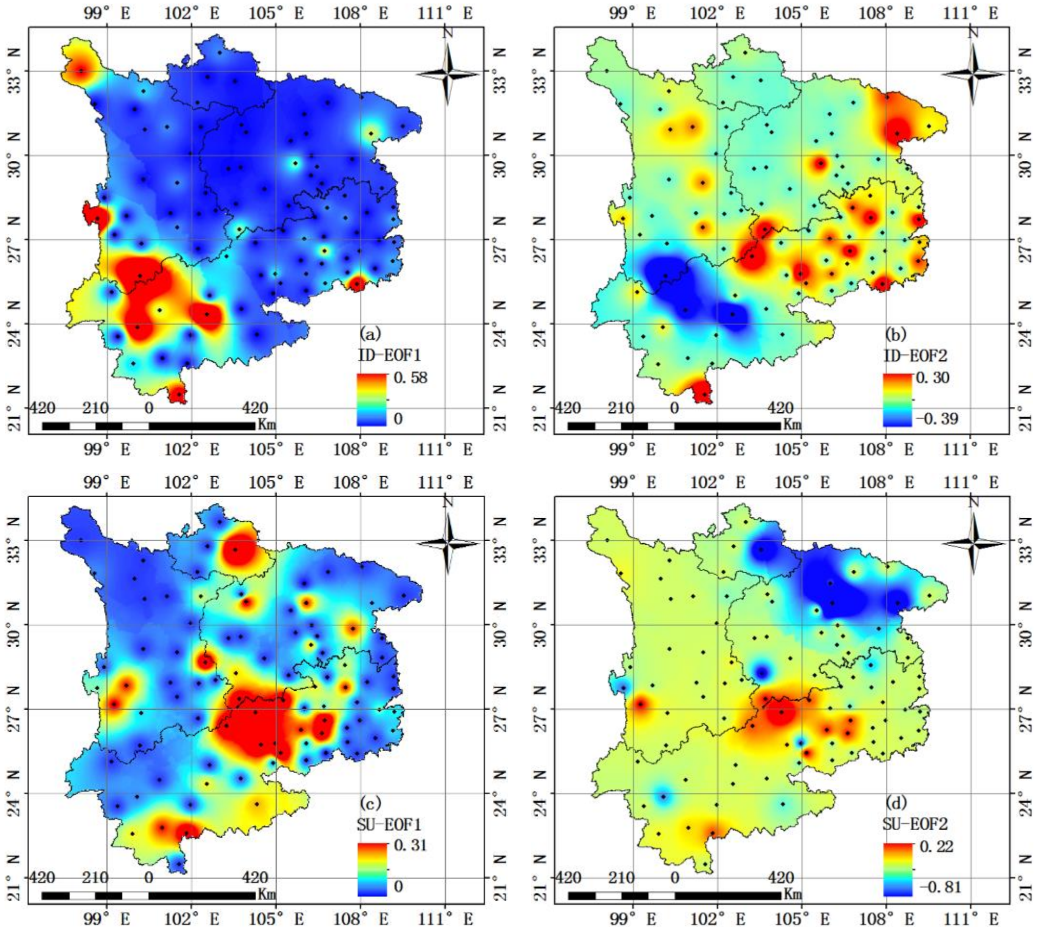

Figure 6. *Spatial EOF variation for ID and SU*

Analysis of the relationship between ETIs and ENSO events

Two indices, SOI and ONI, were chosen for mutual validation in order to prove the occurrence of ENSO events. Further comparisons showed that strong El Niño phenomena (SOI << 0 and ONI >> + 0.5 °C) occurred in the years of 1982, 1987, 1991, 1992, 1997, and 2015. On the other hand, strong La Niña phenomena (SOI >> 0 and ONI << + 0.5 °C) occurred in the years of 1971, 1974, 1975, 1999, 2008, and 2011. Once the composite ETIs rate was calculated, the influence of ENSO events on ETIs was determined, and results are shown in *Table 7*. Data indicated that CSDI was the most affected index as a consequence of ENSO events. The change rate in the El Niño year was -16.86%. That is, the cold spell duration decreased. Furthermore, the change rate increased to 86.68% during La Niña year. The number of cold days during the abnormal years was about twice that of the long-term average number of days. The cold spell duration was considerably extended. FD, ID, TNn, and CSDI values were similar. A descending trend was observed for these indices during El Niño years, while an

http://www.aloki.hu ● ISSN 1589 1623 (Print) ● ISSN 1785 0037 (Online)
DOI: http://dx.doi.org/10.15666/aeer/2002_11131138

ascendant trend was observed in the La Niña years. In other words, warmer temperatures were observed in the El Niño years and colder temperatures in the La Niña years. The amplitude increase in the number of cold days in the La Niña years was significantly higher than the amplitude decrease in the number of cold days during the El Niño years. Both, TN10p and TX10p, showed an increasing trend in the ENSO years, while TMINmean decreased, indicating a temperature reduction. The change in TXn value indicated a warming trend in the El Niño years, and a cooling trend in La Niña years. WSDI, TR, and TMAXmean showed a downward trend in the ENSO years. It was also observed that this reduction was higher in El Niño years than in La Niña years. SU, TN90p, and TX90p decreased in El Niño years; however, they increased in La Niña years. With respect to these indices, the amplitude reduction was much higher than the amplitude increase. In relation to TNx, this index did not show variations in El Niño years. However, it displayed decreasing values during La Niña years. DTR decreased in El Niño years, which indicated that smaller temperature differences occurred during the same day. However, DTR increased in La Niña years, indicating that larger temperature differences were observed during the same day.

Table 7. *Correlation between 17 EPIs (referring to Table 2) and ENSO events in Southwestern China*

Categories	Indices	El Nino compound ratio	Change rates (%)	La Niña compound ratio	Change rates (%)
Extreme cold indices	CSDI	0.83	-16.86%	1.87	86.68%
	FD	0.98	-1.99%	1.06	5.75%
	ID	0.97	-3.00%	1.28	27.87%
	TN10p	1.05	4.83%	1.15	15.44%
	TX10p	1.12	11.81%	1.07	7.44%
	TMINmean	1.00	-0.24%	0.99	-1.44%
	TNn	0.97	-3.09%	1.18	17.66%
	TXn	1.15	15.40%	0.71	-28.94%
Extreme warm indices	WSDI	0.76	-23.59%	0.92	-7.69%
	TR	0.97	-2.98%	0.98	-1.61%
	SU	0.81	-19.48%	1.01	1.24%
	TN90p	0.95	-4.74%	1.03	2.81%
	TX90p	0.89	-11.27%	1.00	0.28%
	TMAXmean	0.99	-0.89%	1.00	-0.23%
	TNx	1.00	0.00%	0.98	-1.52%
	TXx	1.00	-0.41%	0.99	-0.72%
	DTR	0.99	-1.47%	1.01	1.18%

As previously mentioned, ETIs were closely related to ENSO events. In the El Niño years, the number of cold days decreased (-1.04%), while temperature increased (4.03%), as indicated by the extreme cold indices. On the other hand, during La Niña years, the number of cold days increased (28.64%), and temperature decreased (-4.24%). According to values of the extreme warm indices obtained in the present research, the number of warm days during El Niño years decreased (-12.41%), and temperature value was reduced (-0.43%). Moreover, in La Niña years, the number of

http://www.aloki.hu ● ISSN 1589 1623 (Print) ● ISSN 1785 0037 (Online)
DOI: http://dx.doi.org/10.15666/aeer/2002_11131138

warm days decreased (-0.99%), while temperature was reduced (-0.82%). According to these results, the extreme cold indices were more susceptible to the influence of the ENSO events, and the change in amplitude was significantly larger than that observed for extreme warm indices. Thus, La Niña had a greater impact on extreme cold indices, while El Niño displayed a more significant impact on extreme warm indices.

Discussion

(1) According to the interannual ETIs variation (*Fig. 2*), the results on extreme cold indices indicated a warming trend. Similarly, the extreme warm indices showed an increasing trend. Our results agreed with other investigations that determined overall changes in extreme temperatures (a) on a global scale (Alexander et al., 2006); (b) in China (Yang et al., 2010); and Southwestern China (Wang et al., 2014a; Luo et al., 2015; Luo et al., 2016). Most ETIs change trends obtained in the present research were similar to those published by Yuan et al. (2015). However, the amplitude of the change varied slightly depending on the dataset or time scale used. Yuan et al. (2015) reported a significant difference in the amplitude change between different types of ETIs. Specifically, the amplitude change for TN10p and TX90p was greater than that for other ETIs, which was also consistent with our findings. In relation to the spatial trend, the extreme cold indices decreased from west to east. The warming trend was more pronounced in the extreme cold indices in the Hengduan Mountains than in other regions. In addition, the Sichuan Basin and southwestern Yunnan-Guizhou Plateau displayed the extreme warm events with the highest frequency and intensity. According to our results, DTR showed a decreasing trend, indicating a gradual reduction of the daily temperature differences. Similarly to other indices, the results published by Yang et al. (2010) were alike. Thus, even when there are slight differences in climate variability across different geographical divisions, the warming trend seems definite. This means that Southwestern China has been experiencing a warming trend for the past 49 years.

(2) As indicated by the Sen's slope estimator (*Table 5*), the number of cold days in Southwestern China suddenly decreased in the 1990s, and temperature increased. Later, in the early 21st century, an abrupt change in extreme warm indices with a higher number of warm days and higher temperatures occurred. The results of the Sen's slope estimator corroborated the regression coefficients of the interannual and interdecadal ETIs changes, as well as the UF statistics calculated by SPSS. Thus, in Southwestern China, an upward temperature trend has been observed for the past 49 years. In addition, an abrupt change in temperature occurred in the 1990s and the early 21st century (2001-2011). This conclusion was consistent with the data published by Zhu et al. (2018) the region of Guizhou. However, according to He et al. (2011), the amplitude increase in extreme low temperature was significantly higher than that of the extreme high temperature, which was consistent with our findings. Moreover, He et al. (2011) suggested that the abrupt change in the extreme droughts occurred during the monsoon season of 2003 in Southwestern China. Also, the abrupt change in the non-monsoon season occurred in 1989. Even when the methods used by He et al. (2011) differ from ours, the findings were similar. Jia et al. (2018) showed that droughts hit Southwestern China at a higher intensity in the years of 1970 and 2000. Since extreme temperature events usually occur concomitantly with droughts, their results also support our findings.

(3) The results of the EOF analysis also indicated a decrease in the extreme cold indices and an abrupt change in the 1990s. Extreme warm indices increased, and their

http://www.aloki.hu ● ISSN 1589 1623 (Print) ● ISSN 1785 0037 (Online)
DOI: http://dx.doi.org/10.15666/aeer/2002_11131138

abrupt change generally occurred in the early 21st century. Furthermore, regions susceptible to the changes in ID were identified in a small area of the western Hengduan Mountains and in a large area of the western Yunnan-Guizhou Plateau. The high-value centers of SU were found in the eastern Zoige Plateau, part of Sichuan Basin, and the central Yunnan-Guizhou Plateau. These findings also proved the following spatiotemporal characteristics of ETIs in Southwestern China: (a) the warming trend in the extreme cold indices was the highest in the Hengduan Mountains; (b) extreme warm events were more frequent in the Sichuan Basin and southwestern Yunnan-Guizhou Plateau than in the rest of the regions. Wang et al. (2014a, b), who studied the drought events in Southwestern China, found out that droughts were more likely to occur in the Yunnan-Guizhou Plateau and part of the Sichuan Basin. The frequency of droughts was higher in the Zoige Plateau and southwestern Sichuan Basin than in other regions. It was also determined that the Southwestern Yunnan-Guizhou Plateau was susceptible to droughts. These findings support the conclusion that extreme warm events occurred more frequently in the Sichuan Basin and southwestern Yunnan-Guizhou Province, where the susceptibility to droughts was also higher with respect to other regions.

(4) Shi (2017) suggested that ENSO were more intense between 1970s and 1990s. The ENSO geographical range of influence was wider in the north-south direction. The midpoint of maximum anomaly in sea surface temperature was identified in the east. This finding confirmed that the ENSO years selected in the present study were appropriate, and also indicated an upward temperature trend in the ENSO years. Lim and Schubert (2011), Shi et al. (2018) and Moon et al. (2011) all concluded that extreme climate events were associated with the circulation index. These researchers proved that the correlation between ETIs and ENSO events was significant. Wang et al. (2014a) analyzed the correlation between drought events and ENSO events in Southwestern China and identified a correlation between the ENSO index and drought index in a long time series. However, the correlation between these two indices was lower, and the relationship more complex than originally hypothesized. Also, comparing different regions, Sichuan Basin and Zoige Plateau were susceptible to droughts in the El Niño years, while these events were less frequent in La Niña years. However, for the Yunnan-Guizhou Plateau, droughts were more likely to occur in La Niña years. Moreover, the probability of droughts was higher in El Niño years and lower in the La Niña years. The present conclusion corroborated the reliability of our findings. That is, ETIs were correlated to ENSO events. In addition, upward and downward temperature trends were identified in the El Niño and the La Niña years, respectively. Wang et al. (2019) determined that the southeast monsoon was weakened when SOI entered the negative phase and the El Niño phenomenon occurred. They also suggested that large-scale droughts in Southwestern China were related to the El Niño phenomenon and Yunnan-Guizhou Plateau was more vulnerable to the influence of SOI. Existing studies have shown that extreme temperature events are also remotely related to the circulation indices, including the AO (Arctic Oscillation) (Lim et al., 2011), AMO (Atlantic Multidecadal Oscillation), DMI (Dipole Mode Index) (Shi et al., 2018), MJO (Madden–Julian Oscillation) (Moon et al., 2011), and NAO (North Atlantic Oscillation) (Grotjahn, 2011). In addition, in recent years, due to the implementation of the western development strategy and the construction of new urbanization roads in China, the built-up areas of the four provinces and cities in Southwestern China have been expanding and the urbanization process has been accelerated. Cities as areas of concentration of human activities, urban heat island phenomenon will appear in different degrees due to

http://www.aloki.hu ● ISSN 1589 1623 (Print) ● ISSN 1785 0037 (Online)
DOI: http://dx.doi.org/10.15666/aeer/2002_11131138

the change of underlying surface properties and the emission of anthropogenic heat. Many studies also showed that the impact of urbanization on extreme temperature events cannot be ignored (Jiao et al., 2020; Lin et al., 2020).

Conclusions

Extreme weather events refer to a type of rare events that occur at specific sites and at a specific time. The occurrence of extreme weather events can be determined based on the values of extreme indices. In this study, data on daily mean temperatures as well as daily maximum and minimum temperatures were obtained in 93 weather stations in Southwestern China for the period 1969 to 2017. Seventeen ETIs were selected according to the climate indices recommended by the ETCCDMI. These index data were analyzed using linear regression, M-K trend test, Sen's slope estimator, and EOF analysis. In addition, extreme spatiotemporal climate changes for the past 49 years were analyzed. The results of this analysis were used to determine the relationships between: SOI and ONI with ETIs, as well as the correlation between ETIs and ENSO events in Southwestern China. The following conclusions were reached:

(1) during the past 49 years, ETIs showed a warming trend in Southwestern China, which responded positively to global warming. Also, differences in warming trends were observed in different geographical regions. For example, increasing temperatures were more evident in the Hengduan Mountains. In addition, in the Sichuan Basin and southwestern Yunnan-Guizhou Plateau, the extreme warm events occurred more frequently and at a higher intensity as compared to other regions. The diurnal temperature range (DTR) decreased, indicating increasingly small daily temperature differences.

(2) In the 1990s and early 21st century (2001-2011), abrupt temperature changes were observed. While in the 1990s the number of days of extreme cold indices suddenly decreased, in the early 21st century (2001-2008) the extreme warm indices suddenly increased.

(3) Results of the EOF analysis also indicated abrupt changes in temperature indices. The regions susceptible to changes in the number of ice days (ID) were the Hengduan Mountains and part of the Yunnan-Guizhou Plateau. The high-value midpoints of summer days (SU) were found in the Zoige Plateau, Sichuan Basin, and part of the Yunnan-Guizhou plateau.

(4) ETIs were closely related to the ENSO events. The extreme cold indices were more influenced by La Niña, and the extreme warm indices were more susceptible to El Niño events. The amplitude change of the extreme cold indices was more significant than that of the extreme warm indices. The number of days with cold indices consistently decreased, and the temperature increased during the El Niño years. On the other hand, in La Niña years, the number of days with warm indices increased, and temperature decreased. The extreme warm indices showed a decreasing trend in all the ENSO years. However, the amplitude change of some of the indices was negligible. DTR indicated a reduced difference between the daily maximum and minimum temperatures in the El Niño years, and an increased difference in the La Niña years.

Extreme temperature events have important implications for agricultural and livestock production, resource protection and socio-economic development in Southwestern China. However, due to the specificity and complexity of extreme temperature events themselves, their influencing factors involve not only natural factors

http://www.aloki.hu ● ISSN 1589 1623 (Print) ● ISSN 1785 0037 (Online)
DOI: http://dx.doi.org/10.15666/aeer/2002_11131138

but also human factors caused by human activities. The research in this paper only analyzed the characteristics of extreme temperature index changes from the perspective of climate statistics, and explored the causes of influence less, which has certain limitations. In the future, in order to clarify the influencing factors and physical mechanisms of its spatiotemporal change trends, a more in-depth and comprehensive discussion can be conducted from various aspects and perspectives, such as atmospheric circulation anomalies, water vapor transport, solar activity, urbanization process, underlying surface land use changes, and greenhouse gas emissions. At the same time, in order to cope with the future extreme climate risks caused by continuous global warming, an early warning system for extreme temperature events can be established and improved, and CMIP6 model data can be applied to project extreme temperature events in Southwestern China for different scenarios and different time scales, which will be further analyzed and discussed in depth in the future.

Acknowledgements. Thanks to support from foundation of the Second Tibetan Plateau Scientific Expedition and Research Program (2019QZKK0105).

REFERENCES

[1] Alexander, L. V., Zhang, X., Peterson, T. C., Caesar, J., Gleason, B., Klein Tank, A. M. G., Haylock, M., Collins, D., Trewin, B., Rahimzadeh, F., Tagipour, A., Rupa Kumar, K., Revadekar, J., Griffiths, G., Vincent, L., Stephenson, D. B., Burn, J., Aguilar, E., Brunet, M., Taylor, M., New, M., Zhai, P., Rusticucci, M., Vazquez-Aguirre, J. L. (2006): Global observed changes in daily climate extremes of temperature and precipitation. – Journal of Geophysical Research Atmospheres 111: D05109.

[2] An, D., Du, Y. H., Berndtsson, R., Niu, Z. R., Zhang, L., Yuan, F. F. (2019): Evidence of climate shift for temperature and precipitation extremes across Gansu Province in China. – Theoretical and Applied Climatology 139(3-4): 1137-1149.

[3] Cai, W. X. (2016): Temporal Trends Features and Spatial Distributions of Extreme Climate Events in China. – University of International Business and Economics, Beijing.

[4] Chen, D., Min, J. (2017): Analysis on the variation of extreme precipitation indices in the mid-lower Yangtze River valley of China. – Journal of the Meteorological Sciences 37: 497-504.

[5] China Meteorological Administration (2007): China Meteorological Disaster Yearbook. – Meteorological Press, Beijing.

[6] Choi, G. Y., Collins, D., Ren, G. Y., Trewin, B., Baldi, M., Fukuda, Y., Afzaal, M., Pianmana, T., Gomboluudev, P., Huong, P. T. T., Lias, N., Kwon, W. T., Boo, K. O., Cha, Y. M., Zhou, Y. Q. (2009): Changes in means and extreme events of temperature and precipitation in the Asia-Pacific Network Region, 1955-2007. – International Journal of Climatology 29: 1906-1925.

[7] Croitoru, A. E., Chiotoroiu, B. C., Todorova, V. I., Torică, V. (2013): Changes in precipitation extremes on the Black Sea western coast. – Global Planetary Change 102: 10-19.

[8] Cui, F. Q., Tang, H. P., Zhang, Q., Dai, L. W. (2018): Temporal and spatial variations of extreme climatic events in Hulunbuir Grassland, Northeast China during 1960-2017. – Arid Zone Research 35: 1382-1391.

[9] Diffenbaugh, N. S., Singh, D., Mankin, J. S., Horton, D. E., Swain, D. L., Touma, D., Charland, A., Liu, Y. J., Haugen, M., Tsiang, M., Rajaratnam, B. (2017): Quantifying the influence of global warming on unprecedented extreme climate events. – Proceedings of the National Academy of Sciences 114: 4881-4886.

[10] Ding, Z. Y., Ge, Y. Z., Abuduwaili, J., Pu, J. (2018): Trends of extreme temperature and precipitation in Ebinur Lake basin in Xinjiang during the period from 1957 to 2012. – Journal of University of Chinese Academy of Sciences 35: 160-171.
[11] Fu, C. B., Wang, Q. (1992): The definition and detection of the abrupt climate change. – Scientia Atmospherica Sinica 16: 482-493.
[12] Gao, T., Xie, L. (2016): Spatiotemporal changes in precipitation extremes over Yangtze River basin, China, considering the rainfall shift in the late 1970s. – Global and Planetary Change 147: 106-124.
[13] Gao, W. H., Li, K. F., Cui, Y. (2017): Temporal and spatial variation of extreme temperature events in Henan Province during 1960-2014. – Scientia Geographica Sinica 37: 1259-1269.
[14] Glantz, M. H., Wang, S. W., Zhou, T. J., Qian, W. (1998): Currents of Change: EI Nino’s Impact on Climate and Society. – Meteorological Press, Beijing.
[15] Grotjahn, R. (2011): Identifying extreme hottest days from large scale upper air data: a pilot scheme to find California Central Valley summertime maximum surface temperatures. – Climate Dynamics 37: 587-604.
[16] Grotjahn, R., Black, R., Leung, R., Wehner, M., Barlow, M., Bosilovich, M., Gershunov, A., Gutowski Jr, W. J., Gyakum, J. R., Katz, R. W., Lee, Y. Y., Lim, Y. K. (2016): North American extreme temperature events and related large scale meteorological patterns: a review of statistical methods, dynamics, modeling, and trends. – Climate Dynamics 46: 1151-1184.
[17] He, J. Y., Zhang, M. J., Wang, P., Wang, S. J., Wang, X. M. (2011): Climate characteristics of the extreme drought events in Southwest China during recent 50 years. – Acta Geographica Sinica 66: 29-40.
[18] IPCC (2013): Summary for Policymakers. – In: Climate Change 2013: The Physical Science Basis. Contribution of Working Group I to the Fifth Assessment Report of the Intergovernmental Panel on Climate Change. Cambridge University Press, Cambridge.
[19] Jia, Y. Q., Zhang, B., Ma, B., Wu, Q. H. (2018): Spatio-temporal evolution characteristics of persistent drought in Southwest China in 1960-2015. – Journal of Arid Land Resources and Environment 32: 171-176.
[20] Jiang, R. G., Xie, J. C., Zhao, Y., He, H. L., He, G. H. (2017): Spatiotemporal variability of extreme precipitation in Shaanxi Province under climate change. – Theoretical and Applied Climatology 130: 821-845.
[21] Jiao, Y. M., Zhao, N., Yue, T. X., Deng, J. Y. (2020): The effect of urbanization on extreme climate events in Beijing. – Geographical Research 39: 461-472.
[22] Karl, T. R., Kukla, G., Razuvayev, V. N., Changery, M. J., Quayle, R. G., Heim, Jr. R. R., Easterling, D. R., Fu, C. B. (1991): Global warming: evidence for asymmetric diurnal temperature change. – Geophysical Research Letters 18: 2253-2256.
[23] L’Heureux, M. L., Takahashi, K., Watkins, A. B., Barnston, A. G., Becker, E. J., DiLiberto, T. E., Gamble, F., Gottschalck, J., Halpert, M. S., Huang, B., Mosquera-Vasquez, K., Wittenberg, A. T. (2017): Observing and predicting the 2015/16 El Niño. – American Meteorological Society 98: 1363-1382.
[24] Li, J., Zhao, Y. D., Iqbal, J. (2019): Variation patterns of extreme precipitation and relation to ocean-atmospheric climate in Sichuan Province China from 1961 to 2017. – Theoretical and Applied Climatology 137: 3009-3026.
[25] Lim, Y. K., Schubert, S. (2011): The impact of ENSO and the arctic oscillation on winter temperature extremes in the Southeast United States. – Geophysical Research Letters 38: L15706.
[26] Lin, L. J., Gao, T., Luo, M., Ge, E. J., Yang, Y. J., Liu, Z., Zhao, Y. Q., Ning, G. C. (2020): Contribution of urbanization to the changes in extreme climate events in urban agglomerations across China. – Science of the Total Environment 744: 140264.

http://www.aloki.hu ● ISSN 1589 1623 (Print) ● ISSN 1785 0037 (Online)
DOI: http://dx.doi.org/10.15666/aeer/2002_11131138

[27] Liu, L., Xu, Z. X. (2014): Spatiotemporal distribution of the extreme climate indices in the five southwestern provinces of China. – Resources and Environment in the Yangtze Basin 23: 294-301.
[28] Luo, Y., Fang, G. Z., Zhou, D. W., Hua, W., Li, J. J. (2015): Extreme precipitation trend of Southwest China in recent 41 years. – Journal of the Meteorological Sciences 35: 581-586.
[29] Luo, Y., Fan, G. Z., Zhou, D. W., Hua, W., Zhang, Y. L. (2016): Trend of extreme temperature in Southwest China in recent 41 years. – Journal of Southwest University (Natural Science Edition) 38: 161-167.
[30] Ma, R., Zhang, M. J., Wang, S. J., Wang, J., Yang, S., Chen, R. (2018): Variation characteristics of snow cover days in winter in arid region of Northwest China in last 50 years. – Journal of Natural Resources 33: 127-138.
[31] Moon, J. Y., Wang, B., Ha, K. J. (2011): ENSO regulation of MJO teleconnection. – Climate Dynamics 37: 1133-1149.
[32] Peterson, T. C., Zhang, X. B., Brunet-India, M., Vazquez-Aguirre, J. L. (2008): Changes in North American extremes derived from daily weather data. – Journal of Geophysical Research 113: D07113.
[33] Pi, Y. Y., Yu, Y., Zhang, Y. Q., Xu, C. C., Yu, R. D. (2020): Extreme temperature events during 1960–2017 in the arid region of Northwest China: spatiotemporal dynamics and associated large-scale atmospheric circulation. – Sustainability 12: 1198.
[34] Qiu, W. J. (2013): Study on the Influence of Drought on Vegetation Net Primary Productivity in Southwest China. – Shandong Normal University, Shandong.
[35] Shi, H. Y. (2017): Research of ENSO Characteristics Changes during 1900-2015 under Global Warming Background. – Nanjing University of Information Science & Technology, Nanjing.
[36] Shi, J., Cui, L. L., Ma, Y., Du, H. Q., Wen, K. G. (2018): Trends in temperature extremes and their association with circulation patterns in China during 1961–2015. – Atmospheric Research 212: 259-272.
[37] Sponberg, K. (1990): Compendium of Climatological Impacts, University Corporation for Atmospheric Research. Vol. 1. – National Oceanic and Atmospheric Administration, Office of Global Programs, Washington, DC.
[38] State Statistical Bureau (2018): China Statistical Yearbook. – China Statistics Press, Beijing.
[39] Tong, R. Z., Sun, W. C., Han, Q., Yu, J. S., Tian, Z. F. (2020): Spatial and temporal variations in extreme precipitation and temperature events in the Beijing–Tianjin–Hebei Region of China over the past six decades. – Sustainability 12: 1415.
[40] Vincent, L. A., Mekis, É. (2006): Changes in daily and extreme temperature and precipitation indices for Canada over the twentieth century. – Atmosphere-Ocean 44: 177-193.
[41] Wang, D., Zhang, B., An, M. L., Zhang, T. F., Ji, D. M., Ren, P. G. (2014a): Temporal and spatial distributions of drought in Southwest China over the past 53 years based on standardized precipitation evapotranspiration index. – Journal of Natural Resources 29: 1003-1016.
[42] Wang, X. J., Bai, H., Zhou, W. U., Chen, Z. H., Zhang, D. H. (2014b): Comparative analysis of drought in Guizhou from July to August between the year of 2011 and 2013 and the effect on agriculture. – Tianjin Agricultural Sciences 20: 118-124.
[43] Wang, Z. Q., Zhang, W. J., Geng, X. (2017): Different Influences of two types of ENSO on winter temperature and cold extremes in northern China. – Acta Meteorologica Sinica 75: 564-580.
[44] Wang, C. Y., Wan, X. Y. (2019): Independent component analysis of land water changes in Southwest China and Indochina Peninsula. – Geomatics & Spatial Information Technology 42: 43-46.

http://www.aloki.hu ● ISSN 1589 1623 (Print) ● ISSN 1785 0037 (Online)
DOI: http://dx.doi.org/10.15666/aeer/2002_11131138

[45] Wu, J. D., Fu, Y., Zhang, J., Li, N. (2014): Meteorological disaster trend analysis in China: 1949-2013. – Journal of Natural Resources 29: 1520-1530.
[46] Yang, P., Liu, W. D., Wang, Q. G., Xiong, K. G., Hou, W. (2010): The climate change trend and seasonal characteristics of daily temperature extremes in China for the latest 40 years. – Journal of Applied Meteorological Science 21: 29-36.
[47] Yang, D., Wang, H., Cheng, J. Q., Guo, P. P. (2013): Climate change in Qinghai Province and its relationship with ENSO in the recent 50 years. – Ecology and Environmental Sciences 22: 547-553.
[48] Yuan, W. D., Zheng, J. K. (2015): Spatial and temporal variation of extreme temperature events in Southwest China during 1962-2012. – Resources and Environment in the Yangtze Basin 24: 1246-1254.
[49] Zhang, X., Yang, F. (2004): RClimDex 1.1. – http://etccdi.pacificclimate.org/software.shtml.
[50] Zhao, J. (1997): The Physical Geography of China. Fourth Ed. – Higher Education Press, Beijing.
[51] Zhao, A. Z., Liu, X. F., Zhu, X. F., Pan, Y. Z., Zhao, Y. L., Wang, D. L. (2016): Trend variations and spatial difference of extreme air temperature events in the Loess Plateau from 1965 to 2013. – Geographical Research 35: 639-652.
[52] Zhao, A. Z., Zhu, X. F., Pan, Y. Z. (2017): Spatiotemporal variations of extreme precipitation events in the Loess Plateau from 1965 to 2013. – Journal of Beijing Normal University (Natural Science) 53: 43-50.
[53] Zhu, D. Y., Xiong, K. N., Xiao, H. (2018): Analysis of temporal and spatial variation of extreme temperature in Guizhou Province. – Resources Science 40: 1672-1683.

http://www.aloki.hu ● ISSN 1589 1623 (Print) ● ISSN 1785 0037 (Online)
DOI: http://dx.doi.org/10.15666/aeer/2002_11131138